

Long-range permeation of wave function and superficial surface state due to strong quantum size effects in topological Bi/BiSb heterojunctions

Yuya Asaka¹,² Tatsuki Kikuchi,¹ and Yuki Fuseya^{1,2}

¹Department of Engineering Science, University of Electro-Communications, Chofu, Tokyo 182-8585, Japan

²Institute for Advanced Science, University of Electro-Communications, Chofu, Tokyo 182-8585, Japan

(Received 17 August 2022; revised 15 November 2022; accepted 22 November 2022; published 8 December 2022)

The quantum size effect has a significant impact on electrons such that it can even change their topologically protected properties. An example of this phenomenon is the gap opening in the topologically protected gapless surface state in finite-thickness topological-insulator films. However, much is not known about the quantum size effect in topological heterojunctions. In this paper, by calculating the single-particle spectrum of Bi/Bi_{1-x}Sb_x based on the well-known Liu-Allen model, we found that the strong quantum size effect in topological heterojunctions yields an unexpected band alignment. The wave functions permeate each other through the attached materials, and this occurs even in 80-nm-thick heterojunctions. Furthermore, we theoretically found that one of the two major spectra obtained from the Bi surface does not represent the true surface state of Bi. This finding may overturn the previous understanding of the topological surface state of Bi.

DOI: [10.1103/PhysRevB.106.245303](https://doi.org/10.1103/PhysRevB.106.245303)

I. INTRODUCTION

The design and manipulation of heterojunctions, which are interfaces between two dissimilar semiconductors, is one of the most effective ways of controlling band structure. Solar cells, lasers, and high-electron-mobility transistors are examples of successful applications of band engineering via heterojunctions. In general, the band alignment of a heterojunction can be described as a natural connection between the band edges of two semiconductors, as illustrated in Fig. 1(a) [1–3]. In the mid-1980s, the possibility of an interface state (IS) in the gap in a heterojunction between mutually band-inverted semiconductors, such as Pb_{1-x}Sn_xTe [4,5] and Hg_{1-x}Cd_xTe [6–9], was proposed. In recent years, the appearance of the IS has been reexamined in terms of topology. When a topologically nontrivial insulator faces a topologically trivial insulator (including a vacuum), a gapless conducting state must exist at the interface in order to connect bands with the same symmetry as shown in Fig. 1(b) [10,11]. The heterojunction of Pb_{1-x}Sn_xTe and Hg_{1-x}Cd_xTe can be regarded as a topological heterojunction from a contemporary viewpoint [12–16].

The above arguments regarding the topological IS assume an infinite-thickness heterojunction, i.e., a junction between semi-infinite-thickness semiconductors. However, in reality, heterojunctions are fabricated by stacking finite-thickness films. It is naively expected that the band alignment shown in Fig. 1 is discretized owing to the quantum size effect in the heterojunctions of finite thickness. In addition, the quantum size effect changes the topological surface state (SS) of finite-thickness topological insulators [17–21]; the gapless metallic SS in a semi-infinite system produces a gap in the finite-thickness system owing to the interference between the surfaces of the opposite sides. The quantum size effect becomes substantially prominent when the wavelength

of the electrons is increased. Even the topologically protected conditions can be changed by the quantum size effect arising from long-wavelength electrons, such as in Bi_{1-x}Sb_x (BiSb) [21,22]. Similar quantum size effects are expected in topological heterojunctions; the gapless IS of topologically nontrivial heterojunction, Fig. 1(b), may be changed into an ordinary IS of trivial heterojunction, Fig. 1(a). However, it is not clearly understood how the quantum size effect changes the band alignment in topological heterojunctions. Several works have reported the topological “proximity” effect. The topological SS seeped out the attached topologically trivial atomic layer in Zn *M*/Bi₂Se₃ (*M* = S, Se, and Te) [14] and in Bi/TlBiSe₂ [15]. Meanwhile, the interfacial state seeped out the attached topological insulator in Bi₂Se₃/MnSe [23] and in MnBi₂Se₄/Bi₂Se₃ [24]. In these works, however, the penetration of the wave function is limited only in close proximity of ~1 nm. It is difficult to investigate how the quantum size effect affects the band alignment of topological heterojunctions in a such extremely narrow region.

Another type of topological proximity effect can be also observed in the topological superlattice [25]. It is composed of thin films of a magnetically doped topological insulator and ordinary insulator. The proximity effect of wave functions can change the topology of the system.

In this paper, we investigate the “thick” topological heterojunction between Bi and BiSb where the surface, interface, and bulk states are spatially well separated. We demonstrate that the band alignment of the topological heterojunction can be neither Fig. 1(a) nor 1(b), contrary to theoretical expectations. The strong quantum size effect yields an unexpected band alignment [Fig. 2(b)] that cannot be classified into the typical category of heterojunctions [1–3].

The Bi/BiSb heterojunction provides an ideal foundation for investigating the quantum size effect in heterojunctions. Bi is well known for its exceptionally long wavelength

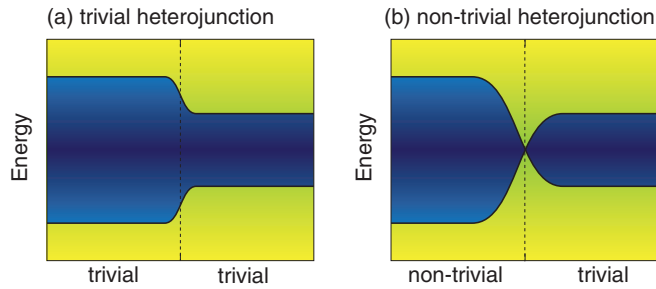


FIG. 1. Schematics of heterojunctions (a) between topologically trivial semiconductors and (b) between trivial and nontrivial semiconductors. In finite-thickness heterojunctions, these band alignments are discretized due to the quantum size effect.

(~ 100 nm) [26–28] that induces a strong quantum size effect [21,22]. Another advantage of this system is that we can control the topology of one side of the junction, BiSb by slightly changing the Sb content, thereby keeping the crystal structure and the lattice constant almost unchanged. It is experimentally well established that the conduction band (CB) and valence band (VB) at the L point in the bulk Brillouin zone are inverted at $x = x_c^{\text{exp}} \simeq 0.04$ [29–33] accompanied by the Z_2 -topological transition [10,34].

II. THEORY

In this paper we investigate Bi/BiSb heterojunctions of a finite thickness [35–42] based on the tight-binding model for bulk Bi and Sb proposed by Liu and Allen [26]; specifically, we focus on (111) films and heterojunctions because (111) is the most easily grown plane, and, thus, the most investigated orientation. The Liu-Allen model provides results that quantitatively agree well with experiments on bulk Bi and Sb [10,11,34]. Similar to that of other band calculations [43,44], the Z_2 topology of pure Bi is trivial in the Liu-Allen model [34,45]. Furthermore, the Liu-Allen model can reproduce the band inversion at the L point and the topological transition by extrapolating the parameters for pure Bi and Sb [21,45,46]. We adopt a simple virtual crystal approximation with a linear extrapolation of tight-binding parameters of pure Bi and Sb

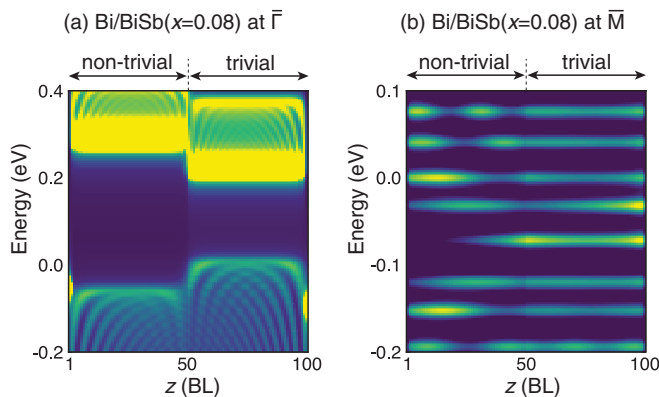


FIG. 2. Present results of topological heterojunction Bi/Bi_{1-x}Sb_x ($x = 0.08$) of 50+50 BL at (a) the $\bar{\Gamma}$ point and (b) the \bar{M} point.

[21,46]. Within this approximation, the topological transition occurs at $x_c = 0.02$ [47], which is less than the experimental value $x_c^{\text{exp}} \simeq 0.04$ [29–33]. The quantitative mismatch can be attributed to the overly simple linear extrapolation. However, this mismatch does not affect the overall quantum size effect findings. The extension of the Liu-Allen model for a finite-thickness film is straightforward [21,48]. There have previously been concerns that the Liu-Allen model cannot provide results that agree with experiments on the (111) surface [45]; however, this problem has already been overcome by Saito *et al.*, who considered the effects of the surface potential gradient [48]. In the following calculation, we adopt their surface hopping terms, which can provide results that agree with the experiments on the SS [cf. Figs. 3(a) and 3(b)] [35–37,40–42]. To examine the heterojunction between n -bilayer Bi and n -bilayer BiSb ($n+n$ BL), we used parameters $z = 1 \rightarrow n$ BL for BiSb and $z = n \rightarrow 2n$ BL for Bi [Fig. 3(d)]. In the following section, we predominantly provide the results for the 50+50 BL (20+20 nm) heterojunction; however, we verified that the results were essentially unchanged up to the 100+100 BL (40+40 nm) system as shown in Sec. III C. Additionally, we determined that there was a minimal effect of the interface potential on the following results [47].

III. RESULTS

Before considering the Bi/BiSb heterojunction, we briefly examined the properties of the (111) surface of free-standing Bi and BiSb. The energy dispersions for free-standing trivial Bi (50 BL) and free-standing nontrivial BiSb (50 BL, $x = 0.08$: deep inside the nontrivial region [47]) are plotted in Figs. 3(a) and 3(b), respectively. The eigenenergies corresponding to the SS are colored in red for Bi and in blue for BiSb. The gray lines correspond to the eigenenergy of the bulk state. There are two SSs between the $\bar{\Gamma}$ - \bar{M} points. (The $\bar{\Gamma}$ (\bar{M}) point in the surface Brillouin zone corresponds to the T (L) point in the bulk Brillouin zone, where holes (electrons) are located [47].) We label the upper energy SS as “S1” and the lower one as “S2” [41]. The lowest CB is labeled “C1.” If the film is infinitely thick, there should be no gap between S1 and S2 at the \bar{M} point for $x < x_c$, whereas the gap opens for $x > x_c$ [21]. Conversely, in the finite-thickness film, the gap (~ 72 meV for free-standing 50 BL Bi) opens because of the interference between the opposite-side surfaces. Consequently, there is no observable difference in the energy dispersion of the SSs between $x < x_c$ and $x > x_c$, even though the bulk CB and VB at the L point are inverted, which is consistent with the analytical solutions for BiSb(111) [21].

A. Sb-content dependence

Here, we investigate the Sb-content (x) dependence of the energy dispersion in the Bi/BiSb heterojunction. Figure 3(c) shows the energy dispersion of the SS at the Bi surface [Fig. 3(d)] of the 50+50 BL heterojunction for $x = 0-0.08$. Only the parameters in the BiSb region, i.e., the blue region in Fig. 3(d), were varied. Nevertheless, the SS at the Bi surface exhibits an x dependence despite the fact that none of the parameters in the Bi region were changed [the red region in Fig. 3(d)]. This x dependence clearly indicates that the SS at the Bi surface is affected by the BiSb region, although they are

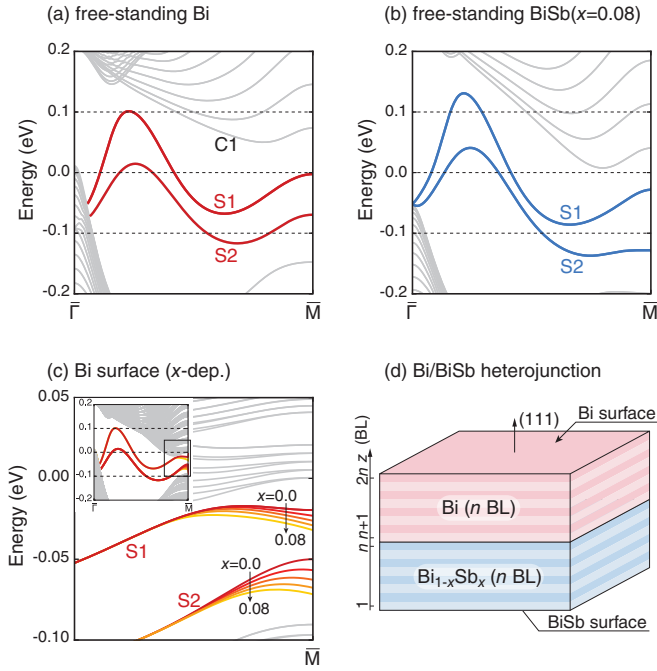


FIG. 3. Energy dispersion of (a) free-standing Bi (50 BL) and (b) free-standing BiSb ($x = 0.08$) (50 BL). (BL denotes bilayer.) (c) x dependence of the SS on the Bi surface of Bi/BiSb ($x = 0.08$) (50+50 BL) around the \bar{M} point. The inset shows the x dependence of the entire $\bar{\Gamma}$ - \bar{M} region. (d) Schematic of the Bi/BiSb heterojunction ($n + n$ BL).

separated by more than 50 BL (≈ 20 nm). It is worth noting that the SS away from the \bar{M} point does not exhibit any x dependence as shown in the inset of Fig. 3(c).

Figure 4 shows the x dependence of the probability distribution $|\psi(z)|^2$ for (a) S1, (b) S2, and (c) C1 in Bi/BiSb (50 + 50 BL). The properties of $|\psi(z)|^2$ change from trivial ($x \lesssim x_c$) to nontrivial ($x \gtrsim x_c$), although the topological transition is smeared due to the finite thickness. For $x \lesssim x_c$ (trivial/trivial), $|\psi(z)|^2$ of S1 and S2 exhibit peaks (the bright region) at the Bi surface ($z = 100$ BL) and the BiSb surface ($z = 1$ BL).

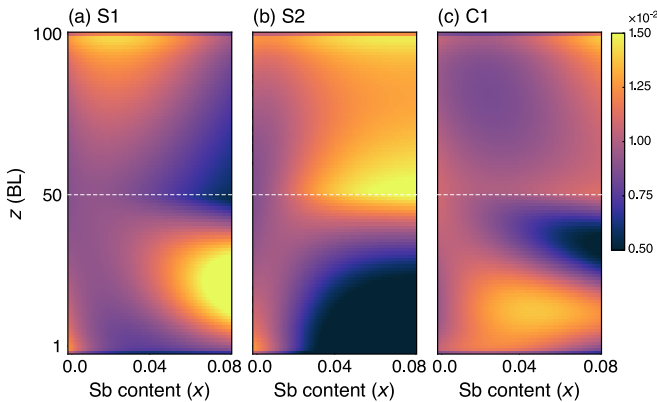


FIG. 4. Probability distribution $|\psi(z)|^2$ for (a) S1, (b) S2, and (c) C1 in Bi/BiSb (50+50 BL). At the BiSb surface ($z = 1$ BL) of S1 and S2, the surface state appears for $x \lesssim x_c$ (≈ 0.02) but does not for $x \gtrsim x_c$, indicating a topological transition.

These peaks are regarded as the SSs of the heterojunction. There is no peak near the interface ($z = 50$ BL). Therefore, the system behaves as if it is a homogeneous 100 BL system. Meanwhile, for $x \gtrsim x_c$ (trivial/nontrivial), the peak of $|\psi(z)|^2$ at the BiSb surface disappears, and the peak appears at the interface in S2, i.e., IS appears. The disappearance of the peak at the BiSb surface for $x > x_c$ is fully consistent with the analytical solution [21]. The appearance of the IS for $x \gtrsim x_c$ is also consistent with the intuitive picture elucidated in the Introduction, and, therefore, these results seem reasonable. However, there is one unexpected property: the IS appears in S2 but not in S1. We will reveal the origin of this unexpected property later.

B. Spatial dependence

The nature of the SS and the IS can be understood more intuitively if we consider the single-particle spectrum $A(\mathbf{k}_{\parallel}, z, \varepsilon)$. Contrary to the eigenvalues (Fig. 3), the spatial (z) dependence can be resolved from $A(\mathbf{k}_{\parallel}, z, \varepsilon)$. Furthermore, $A(\mathbf{k}_{\parallel}, z, \varepsilon)$ directly corresponds to angle-resolved photoemission spectroscopy (ARPES) measurements, making the comparison between theory and experiment more straightforwardly. The single-particle spectrum is calculated based on the standard definition of the form

$$A(\mathbf{k}_{\parallel}, z, \varepsilon) = -\frac{1}{\pi} \text{Tr} \text{Im} G(\mathbf{k}_{\parallel}, z, \varepsilon), \quad (1)$$

$$G(\mathbf{k}_{\parallel}, z, \varepsilon) = [\varepsilon - \mathcal{H}(\mathbf{k}_{\parallel}, z) + i\Sigma'']^{-1}, \quad (2)$$

where G is the Green's function and Σ'' is the imaginary part of the self-energy, which is set to $\Sigma'' = 0.01$ eV in this paper. (The real part of the self-energy is already included in the Hamiltonian \mathcal{H} .) The trace is taken over the Hamiltonian of one BL of interest, which consists of 16 bases of s - and p -orbitals ($s_{\uparrow\downarrow}, p_{x\uparrow\downarrow}, p_{y\uparrow\downarrow}, p_{z\uparrow\downarrow} \times 2 = 16$ bases). The local spectra of Bi/BiSb ($x = 0.08$) are plotted in Ref. [47] for both the Bi surface ($z = 100$ BL) and the BiSb surface ($z = 1$ BL), which perfectly match with those obtained from the eigenvalues of \mathcal{H} .

The band alignment can be microscopically calculated from the z dependence of the single-particle spectrum, which is plotted in Fig. 2 for (a) $\mathbf{k}_{\parallel} = \bar{\Gamma}$ and (d) $\mathbf{k}_{\parallel} = \bar{M}$. We observe from Fig. 2(a) that the band alignment at the $\bar{\Gamma}$ point agrees well with the typical band alignment of the conventional heterojunction, Fig. 1(a). This is reasonable because there is no band inversion at the $\bar{\Gamma}$ point (the T point in bulk). However, the band alignment at the \bar{M} point [Fig. 2(b)] where the band inversion occurs in bulk is entirely different from that is expected as in Figs. 1(a) and 1(b). Each band does not bend around the interface but exhibits flat energy levels without any z dependence. To clarify the origin of this unexpected property of $A(\bar{M}, z, \varepsilon)$, we compared the $A(\bar{M}, z, \varepsilon)$ of the Bi/BiSb heterojunction with that of free-standing Bi and BiSb as shown in Fig. 5, which provided the most significant results of this paper. Notably, we found that each energy level of Bi/BiSb coincides with that of the free-standing Bi and BiSb, whereas alternating between Bi and BiSb. This correspondence shows that the wave functions of the BiSb region permeate those of the Bi region and vice versa. The wave functions of each slab are not connected as is expected from

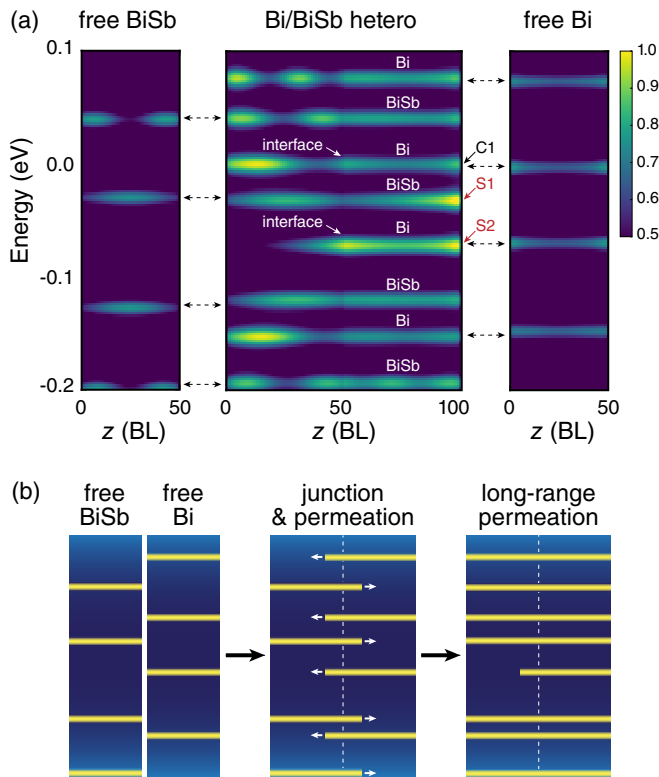


FIG. 5. (a) Comparison of $A(\vec{M}, z, \epsilon)$ of the Bi/BiSb heterojunction and free-standing Bi and BiSb. (For the free-standing Bi and BiSb, the magnitude of A is reduced by 1/2 because their thickness is half that of the Bi/BiSb heterojunction.) (b) Schematic of the permeation in the heterojunction.

Fig. 1(b), but they penetrate the opposite side and retain their energy with no influence from the joined slab. A schematic of the long-range permeation is depicted in Fig. 5(b). From this comparison, it is obvious that S1 on the Bi surface originates from the eigenenergy of BiSb and that the wave function of S2 permeates deeply into the BiSb region. Consequently, both S1 and S2 at the Bi surface are affected by increasing x , which provides a reasonable interpretation of the x dependence of S1 and S2 as shown in Fig. 3(c). Interestingly, the x dependence of $A(\vec{M}, z, \epsilon)$ on the Bi surface perfectly matches that on the BiSb surface, except for the disappearance of the SS on the BiSb surface as shown in Ref. [47]. This correspondence indicates the strong correlation between the Bi and the BiSb surfaces (their correlation length can be 80 nm [47]) due to the exceptionally long-range permeation.

The long-range permeation is realized by the long Fermi wavelength (~ 100 nm) of electrons at the \vec{M} point. Meanwhile, the wavelength of holes at the $\vec{\Gamma}$ point is not so long (~ 10 nm). Consequently, no clear permeation is realized at the $\vec{\Gamma}$ point as shown in Fig. 2(a); this is expected from the ordinary band alignment shown in Fig. 1(a). The difference in the wavelength originates from the anisotropy of the effective mass: $m^*/m_0 = 0.00585$ for electrons at the \vec{M} point and $m^*/m_0 = 0.721$ for holes at the $\vec{\Gamma}$ point [27].

It is not surprising that the mutual permeation of the wave function occurs in the case where the energy levels of one side are almost equal to those of the other, such as $x \lesssim x_c$.

In the case where the energy levels are clearly different from each other, such as $x = 0.08$, it is naively expected that the energy levels of one side naturally continue to the other by bending the energy level at the interface. However, no such level bending was observed. Instead, the energy levels permeate with each other, maintaining the energy levels constant without bending. This is an unexpected result.

It is worth noting that the previously reported topological “proximity” effect [14,15,23,24] could be understood as the precursor of this permeating wave function. However, the previously observed permeation is extremely short range, less than 1.5 nm. In contrast, our results clearly demonstrate that much longer-range permeation (as long as 40 nm as shown later) of the wave functions occurs in thick topological heterojunctions.

The IS, a distinct intensity at the interface $z = 50$ BL, appears not only in S2, but also in C1 (the level just above S1) as shown in Fig. 5(a), which is consistent with Fig. 4(c). Both S2 and C1 originate from the Bi wave function. As is clear from Fig. 5, the appearance of the IS cannot be due to what would be expected from Fig. 1(b). Instead, the IS in S2 and C1 should be interpreted as the SSs of the 50 BL Bi. Based on this understanding, it is reasonable to infer that the S1 does not have an IS (a distinct intensity at the interface) because it originates from BiSb, which does not have SSs due to the topological restriction for $x > x_c$. This provides the solution to the unpredicted lack of an IS in S1.

From Fig. 5, we can obtain information regarding another important property of Bi/BiSb. Suppose the scenario of the ARPES of the Bi *surface* with BiSb as a substrate. We will clearly observe two SSs—S1 and S2—in the ARPES spectrum. We may interpret both S1 and S2 as the SSs of Bi. However, S1 does not appear in the free-standing Bi. S1 appears because of the substrate of BiSb. In this sense, S1 is not the true SS of Bi, but is instead the “superficial” SS originating from the substrate BiSb due to the long-range permeation.

Our scenario of the long-range permeation would be applicable to heterojunctions that have long wavelengths comparable to Bi. Here, we briefly examine two different types of topological heterojunctions TlBiTe₂/InBiTe₂ and Bi₂Te₃/Bi. TlBiTe₂ has Dirac-like electrons at the Γ point [49,50]. The situation is similar to the L point of Bi. Therefore, the permeation of the wave function and superficial SS may be observed even in TlBiTe₂/InBiTe₂. However, the effect is expected to be less significant than Bi/BiSb because the wavelength of TlBiTe₂ is much shorter than that of Bi [49–51]. The heterojunction of Bi₂Te₃/Bi indicates another interesting aspect. The large band gap at the \vec{M} point of Bi₂Te₃ may prevent the Bi electrons from permeating into the Bi₂Te₃ side [52]. However, according to our observation, the Bi electrons can permeate into the attached substance owing to its long wavelength, even if there are no corresponding energy levels. Therefore, a competition between blocking of the Bi₂Te₃ side and permeation from the Bi side will occur, which would be an interesting future problem.

C. Thickness dependence

The single-particle spectra $A(\vec{k}_{\parallel}, z, \epsilon)$ at $\vec{k}_{\parallel} = \vec{M}$ for different thicknesses from 50+50 to 250+250 BL are shown in

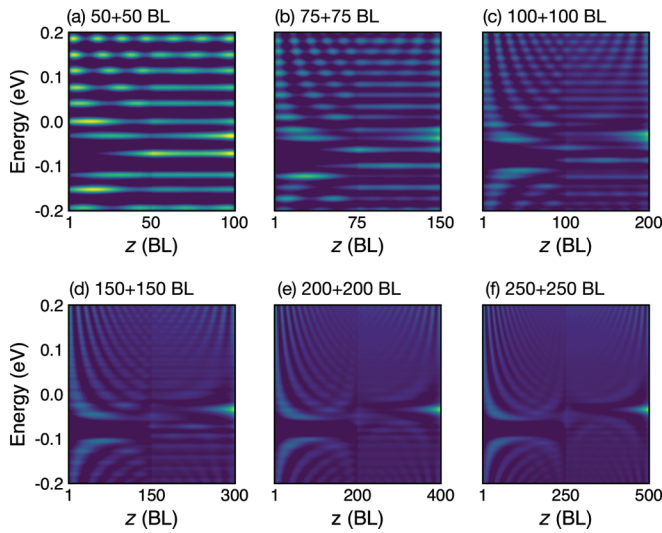


FIG. 6. Single-particle spectrum $A(\bar{M}, z, \varepsilon)$ of Bi/BiSb($x=0.08$) from (a) 50+50 BL to (f) 250+250 BL.

Fig. 6. The long-range permeation where the eigenenergy is common between the Bi ($z > n$) and the BiSb regions ($z \leq n$) is observed for 50+50, 75+75, and 100+100 BL. In contrast, the eigenenergy in the Bi region is different from that in the BiSb region for 200+200 and 250+250 BL. The long-range permeation is not observed for $n \geq 200$ BL. Bi/BiSb of 150+150 BL is the marginal between the permeated and the nonpermeated heterojunctions.

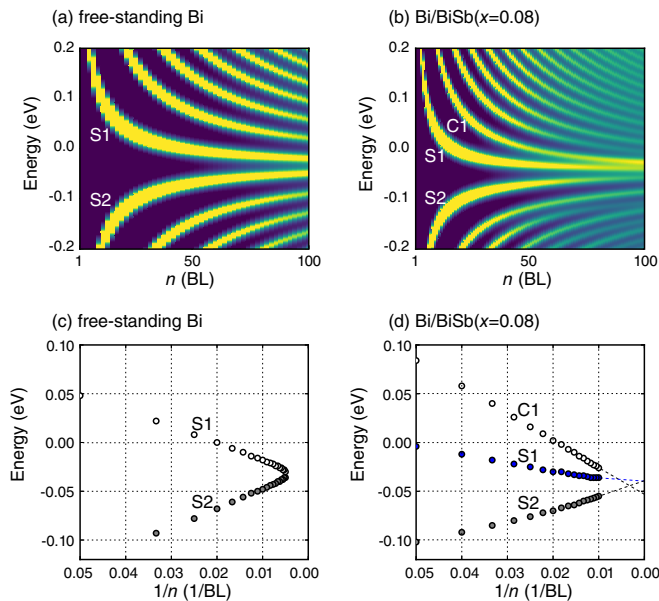


FIG. 7. Thickness dependence of $A(\bar{M}, z, \varepsilon)$ at the Bi surface for (a) free-standing Bi (n BL) and (b) Bi/BiSb ($x = 0.08$) ($n + n$ BL) where the color bar is similar to that in Fig. 5. Their peak positions are plotted as a function of $1/n$ for S1, S2, and C1 in (c) free-standing Bi and (d) Bi/BiSb ($x = 0.08$). The dashed lines in (d) are the extrapolated lines obtained by the least-squares method for thick layers ($n \geq 80$ BL).

The spectrum for 250+250 [Fig. 6(f)] shows the subtle connection between the bottom CB of BiSb and the top VB of Bi. This connection may be an indication of the band connection as expected in the topological heterojunction, Fig. 1(b). However, another side connection between the top VB of BiSb and the bottom CB of Bi is not observed. The band cross expected in the topological heterojunction has not been observed even for thick films.

The unusual behavior of S1, the superficial SS, can be more clearly noted in the thickness dependence. Figure 7 shows the thickness (n) dependence of $A(\bar{M}, z, \varepsilon)$ of the Bi side surface at the \bar{M} point for (a) the free-standing Bi and (b) heterojunction Bi/BiSb. The peak positions of S1 and S2 are plotted as a function of $1/n$ in Fig. 7(c) for the free-standing Bi. The thickness dependences of S1 and S2 are almost symmetric with respect to the center of the band gap for the free-standing Bi. The symmetry between S1 and S2 is a characteristic property of Dirac electrons [21]. Furthermore, it is obvious that the surface gap between S1 and S2 seems to close for $n = 200$ – 300 BL reflecting the topologically trivial characteristic.

However, the symmetry between S1 and S2 is broken in the Bi surface of Bi/BiSb. Furthermore, the gap between S1 and S2 is more significant than in the free-standing Bi, and it will never close around $n = 200$ – 300 BL. This symmetry breaking

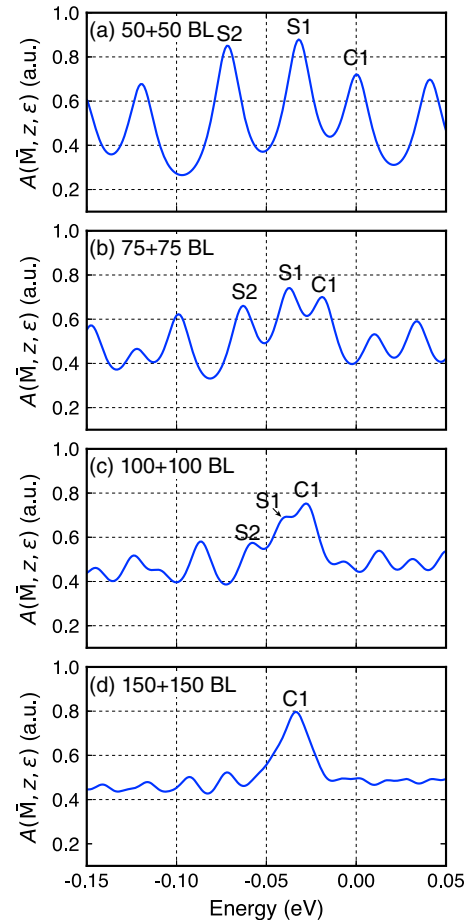


FIG. 8. Single-particle spectrum at the Bi surface for the \bar{M} point, $A(\bar{M}, 2n, \varepsilon)$, from (a) 50+50 BL to (d) 150+150 BL.

and gap opening can be easily understood by considering that S1 originates from the BiSb region. Therefore, we must consider C1 (not S1) to obtain true information regarding the Bi surface. In fact, the thickness dependence of S2 is more symmetric with C1, and the gap between C1 and S2 will close around $n = 200\text{--}300$; both of these findings are consistent with the properties of free-standing Bi. These results provide an important means for the analysis of the SS of Bi. When one measures the surface states using ARPES, S1 and S2 will exhibit the greatest intensity for thin heterojunction, such as 50+50 BL. However, evaluation of the gap based on S1 and S2 will lead to a wrong judgment regarding the topology. One should evaluate the gap based on C1 and S2 in order to obtain the true property of the Bi surface, which will provide us with the accurate topological property. It is worth noting that the asymmetry of the thickness dependence between the two SSs has been observed in pure Bi deposited on a Ge substrate [42]. Although our results cannot be directly applied to their system because of the different substrate, the asymmetry between the SSs observed in the experiment may be related to the superficial SS affected by the substrate.

Figure 8 shows the detailed spectra of $A(\bar{M}, z, \varepsilon)$ from 50+50 BL to 150+150 BL. In thin films of 50+50 BL, the intensity of S1 is larger than C1. By increasing the thickness, the intensity of S1 reduces, whereas that of C1 enhances. In the 100 + 100 BL, the intensity of C1 becomes larger than S1, and the S1 peak is absorbed into the C1 peak. For thick heterojunctions, $n \gtrsim 150$, only the C1 peak survives. This is

another evidence that C1 is the true SS that survives, and S1 is the superficial SS that disappears in the bulk limit.

IV. SUMMARY

We have investigated the quantum size effects in the heterojunction Bi/BiSb where the wavelength of the electrons is large. We found an unexpected band alignment, whereby the wave functions of the electrons permeate through each other. The wave functions of the two substances coexist throughout the entire heterodevice, even though the substances are spatially separated.

Additionally, we found that one of the two major spectra on the Bi side surface S1 was not the true SS of Bi. S1 is the superficial SS originating from the BiSb region, which is far away from the Bi surface. To obtain the true characteristic of the Bi surface, one should consider C1, which is just above S1. Our results strongly suggest that the SS can be drastically affected by the substrate when the wavelength is large, even when a thick film (~ 40 nm) is used.

ACKNOWLEDGMENT

We thank T. Hirahara, L. Perfetti, I. Matsuda, Y. Ohtsubo, A. Takayama, and S. Ito for the fruitful discussions. This work was supported by the Japan Society for the Promotion of Science [Grants No. 19H01850 and No. 22K18318].

-
- [1] C. Kittel, *Introduction to Solid State Physics* (Wiley, Hoboken, NJ, 2005).
 - [2] T. Ihn, *Semiconductor Nanostructures: Quantum States and Electronic Transport* (Oxford University Press, Oxford, 2010).
 - [3] G. Bastard, F. Carosella, and C. Ndebeka-bandou, *Quantum States And Scattering In Semiconductor Nanostructures*, Advanced Textbooks In Physics (World Scientific, Singapore, 2017).
 - [4] B. A. Volkov and O. A. Pankratov, Two-dimensional massless electrons in an inverted contact, *JETP Lett.* **42**, 178 (1985).
 - [5] E. Fradkin, E. Dagotto, and D. Boyanovsky, Physical Realization of the Parity Anomaly in Condensed Matter Physics, *Phys. Rev. Lett.* **57**, 2967 (1986).
 - [6] N. A. Cade, Quantum well bound states of HgTe in CdTe, *J. Phys. C* **18**, 5135 (1985).
 - [7] Y.-C. Chang, J. N. Schulman, G. Bastard, Y. Guldner, and M. Voos, Effects of quasi-interface states in hgte-cdte superlattices, *Phys. Rev. B* **31**, 2557 (1985).
 - [8] Y. R. Lin-Liu and L. J. Sham, Interface states and subbands in hgte-cdte heterostructures, *Phys. Rev. B* **32**, 5561 (1985).
 - [9] O. Pankratov, S. Pakhomov, and B. Volkov, Supersymmetry in heterojunctions: Band-inverting contact on the basis of pb1-xsnxte and hg1-xcdxte, *Solid State Commun.* **61**, 93 (1987).
 - [10] M. Z. Hasan and C. L. Kane, *Colloquium: Topological insulators*, *Rev. Mod. Phys.* **82**, 3045 (2010).
 - [11] X.-L. Qi and S.-C. Zhang, Topological insulators and superconductors, *Rev. Mod. Phys.* **83**, 1057 (2011).
 - [12] B. A. Bernevig, T. L. Hughes, and S.-C. Zhang, Quantum spin hall effect and topological phase transition in hgte quantum wells, *Science* **314**, 1757 (2006).
 - [13] T. H. Hsieh, H. Lin, J. Liu, W. Duan, A. Bansil, and L. Fu, Topological crystalline insulators in the snite material class, *Nat. Commun.* **3**, 982 (2012).
 - [14] G. Wu, H. Chen, Y. Sun, X. Li, P. Cui, C. Franchini, J. Wang, X.-Q. Chen, and Z. Zhang, Tuning the vertical location of helical surface states in topological insulator heterostructures via dual-proximity effects, *Sci. Rep.* **3**, 1233 (2013).
 - [15] T. Shoman, A. Takayama, T. Sato, S. Souma, T. Takahashi, T. Oguchi, K. Segawa, and Y. Ando, Topological proximity effect in a topological insulator hybrid, *Nat. Commun.* **6**, 6547 (2015).
 - [16] G. Krizman, B. A. Assaf, M. Orlita, G. Bauer, G. Springholz, R. Ferreira, L. A. de Vaulchier, and Y. Guldner, Interaction between interface and massive states in multivalley topological heterostructures, *Phys. Rev. Res.* **4**, 013179 (2022).
 - [17] B. Zhou, H.-Z. Lu, R.-L. Chu, S.-Q. Shen, and Q. Niu, Finite Size Effects on Helical Edge States in a Quantum Spin-Hall System, *Phys. Rev. Lett.* **101**, 246807 (2008).
 - [18] J. Linder, T. Yokoyama, and A. Sudbø, Anomalous finite size effects on surface states in the topological insulator bi_2se_3 , *Phys. Rev. B* **80**, 205401 (2009).
 - [19] H.-Z. Lu, W.-Y. Shan, W. Yao, Q. Niu, and S.-Q. Shen, Massive dirac fermions and spin physics in an ultrathin film of topological insulator, *Phys. Rev. B* **81**, 115407 (2010).
 - [20] S.-Q. Shen, *Topological Insulators* (Springer-Verlag, Berlin/Heidelberg, 2012).

- [21] Y. Fuseya and H. Fukuyama, Analytical solutions for the surface states of $\text{bi}_{1-x}\text{sb}_x$, *J. Phys. Soc. Jpn.* **87**, 044710 (2018).
- [22] I. Aguilera, H.-J. Kim, C. Friedrich, G. Bihlmayer, and S. Blügel, z_2 topology of bismuth, *Phys. Rev. Mater.* **5**, L091201 (2021).
- [23] S. V. Eremeev, V. N. Men'shov, V. V. Tugushev, P. M. Echenique, and E. V. Chulkov, Magnetic proximity effect at the three-dimensional topological insulator/magnetic insulator interface, *Phys. Rev. B* **88**, 144430 (2013).
- [24] T. Hirahara, S. V. Eremeev, T. Shirasawa, Y. Okuyama, T. Kubo, R. Nakanishi, R. Akiyama, A. Takayama, T. Hajiri, S.-i. Ideta, M. Matsunami, K. Sumida, K. Miyamoto, Y. Takagi, K. Tanaka, T. Okuda, T. Yokoyama, S.-i. Kimura, S. Hasegawa, and E. V. Chulkov, Large-gap magnetic topological heterostructure formed by subsurface incorporation of a ferromagnetic layer, *Nano Lett.* **17**, 3493 (2017).
- [25] A. A. Burkov and L. Balents, Weyl Semimetal in a Topological Insulator Multilayer, *Phys. Rev. Lett.* **107**, 127205 (2011).
- [26] Y. Liu and R. E. Allen, Electronic structure of the semimetals bi and sb, *Phys. Rev. B* **52**, 1566 (1995).
- [27] Z. Zhu, B. Fauqué, Y. Fuseya, and K. Behnia, Angle resolved landau spectrum of electrons and holes in bismuth, *Phys. Rev. B* **84**, 115137 (2011).
- [28] Y. Fuseya, M. Ogata, and H. Fukuyama, Transport properties and diamagnetism of dirac electrons in bismuth, *J. Phys. Soc. Jpn.* **84**, 012001 (2015).
- [29] L. S. Lerner, K. F. Cuff, and L. R. Williams, Energy-band parameters and relative band-edge motions in the bi-sb alloy system near the semimetal-semiconductor transition, *Rev. Mod. Phys.* **40**, 770 (1968).
- [30] E. Tichovolsky and J. Mavroides, Magnetoreflexion studies on the band structure of bismuth-antimony alloys, *Solid State Commun.* **7**, 927 (1969).
- [31] N. B. Brandt, Y. G. Ponomarev, and S. M. Chudinov, Investigation of the gapless state in bismuth-antimony alloys, *J. Low Temp. Phys.* **8**, 369 (1972).
- [32] G. Oelgart and R. Herrmann, Cyclotron masses in semiconducting $\text{bi}_{1-x}\text{sb}_x$ alloys, *Phys. Status Solidi B* **75**, 189 (1976).
- [33] B. Lenoir, M. Cassart, J.-P. Michenaud, H. Scherrer, and S. Scherrer, Transport properties of Bi-rich Bi-Sb alloys, *J. Phys. Chem. Solids* **57**, 89 (1996).
- [34] L. Fu and C. L. Kane, Topological insulators with inversion symmetry, *Phys. Rev. B* **76**, 045302 (2007).
- [35] C. R. Ast and H. Höchst, Electronic structure of a bismuth bilayer, *Phys. Rev. B* **67**, 113102 (2003).
- [36] Y. M. Koroteev, G. Bihlmayer, J. E. Gayone, E. V. Chulkov, S. Blügel, P. M. Echenique, and P. Hofmann, Strong Spin-Orbit Splitting on Bi Surfaces, *Phys. Rev. Lett.* **93**, 046403 (2004).
- [37] T. Hirahara, T. Nagao, I. Matsuda, G. Bihlmayer, E. V. Chulkov, Y. M. Koroteev, P. M. Echenique, M. Saito, and S. Hasegawa, Role of Spin-Orbit Coupling and Hybridization Effects in the Electronic Structure of Ultrathin Bi Films, *Phys. Rev. Lett.* **97**, 146803 (2006).
- [38] H. Guo, K. Sugawara, A. Takayama, S. Souma, T. Sato, N. Satoh, A. Ohnishi, M. Kitaura, M. Sasaki, Q.-K. Xue, and T. Takahashi, Evolution of surface states in $\text{bi}_{1-x}\text{sb}_x$ alloys across the topological phase transition, *Phys. Rev. B* **83**, 201104(R) (2011).
- [39] F. Nakamura, Y. Kousa, A. A. Taskin, Y. Takeichi, A. Nishide, A. Kakizaki, M. D'Angelo, P. Lefevre, F. Bertran, A. Taleb-Ibrahimi, F. Komori, S.-i. Kimura, H. Kondo, Y. Ando, and I. Matsuda, Topological transition in $\text{bi}_{1-x}\text{sb}_x$ studied as a function of sb doping, *Phys. Rev. B* **84**, 235308 (2011).
- [40] Y. Ohtsubo, L. Perfetti, M. O. Goerbig, P. L. Fevre, F. Bertran, and A. Taleb-Ibrahimi, Non-trivial surface-band dispersion on $\text{bi}(111)$, *New J. Phys.* **15**, 033041 (2013).
- [41] H. M. Benia, C. Straßer, K. Kern, and C. R. Ast, Surface band structure of $\text{Bi}_{1-x}\text{Sb}_x(111)$, *Phys. Rev. B* **91**, 161406(R) (2015).
- [42] S. Ito, B. Feng, M. Arita, A. Takayama, R.-Y. Liu, T. Someya, W.-C. Chen, T. Iimori, H. Namatame, M. Taniguchi, C.-M. Cheng, S.-J. Tang, F. Komori, K. Kobayashi, T.-C. Chiang, and I. Matsuda, Proving Nontrivial Topology of Pure Bismuth by Quantum Confinement, *Phys. Rev. Lett.* **117**, 236402 (2016).
- [43] S. Golin, Band structure of bismuth: Pseudopotential approach, *Phys. Rev.* **166**, 643 (1968).
- [44] I. Aguilera, C. Friedrich, and S. Blügel, Electronic phase transitions of bismuth under strain from relativistic self-consistent *gw* calculations, *Phys. Rev. B* **91**, 125129 (2015).
- [45] J. C. Y. Teo, L. Fu, and C. L. Kane, Surface states and topological invariants in three-dimensional topological insulators: Application to $\text{bi}_{1-x}\text{sb}_x$, *Phys. Rev. B* **78**, 045426 (2008).
- [46] Y. Fuseya, Z. Zhu, B. Fauqué, W. Kang, B. Lenoir, and K. Behnia, Origin of the large anisotropic *g* factor of holes in bismuth, *Phys. Rev. Lett.* **115**, 216401 (2015).
- [47] See Supplemental Material at <http://link.aps.org/supplemental/10.1103/PhysRevB.106.245303> for details.
- [48] K. Saito, H. Sawahata, T. Komine, and T. Aono, Tight-binding theory of surface spin states on bismuth thin films, *Phys. Rev. B* **93**, 041301(R) (2016).
- [49] Y. L. Chen, Z. K. Liu, J. G. Analytis, J.-H. Chu, H. J. Zhang, B. H. Yan, S.-K. Mo, R. G. Moore, D. H. Lu, I. R. Fisher, S. C. Zhang, Z. Hussain, and Z.-X. Shen, Single Dirac Cone Topological Surface State and Unusual Thermoelectric Property of Compounds from a New Topological Insulator Family, *Phys. Rev. Lett.* **105**, 266401 (2010).
- [50] S. V. Eremeev, G. Bihlmayer, M. Vergniory, Y. M. Koroteev, T. V. Menshchikova, J. Henk, A. Ernst, and E. V. Chulkov, Ab initio electronic structure of thallium-based topological insulators, *Phys. Rev. B* **83**, 205129 (2011).
- [51] K. M. Paraskevopoulos, Electron effective mass dependence on carrier concentration in tibite_2 monocrystals, *Phys. Status Solidi B* **127**, K45 (1985).
- [52] M. Michiardi, I. Aguilera, M. Bianchi, V. E. de Carvalho, L. O. Ladeira, N. G. Teixeira, E. A. Soares, C. Friedrich, S. Blügel, and P. Hofmann, Bulk band structure of Bi_2Te_3 , *Phys. Rev. B* **90**, 075105 (2014).